Passive Millimeter Wave Imaging and Spectroscopy System for Terrestrial Remote Sensing

Nachappa Gopalsami, Shaolin Liao, Eugene R. Koehl, Thomas W. Elmer, Alexander Heifetz, Hual-Te Chien, Apostolos C. Raptis
Argonne National Laboratory, 9700 S. Cass Avenue, Lemont, IL, USA 60439-4872

ABSTRACT

We have built a passive millimeter wave imaging and spectroscopy system with a 15-channel filter bank in the 146-154 GHz band for terrestrial remote sensing. We had built the spectroscopy system first and have now retrofitted an imaging element to it as a single pixel imager. The imaging element consisted of a 15-cm-diameter imaging lens fed to a corrugated scalar horn. Image acquisition is carried out by scanning the lens with a 2-axis translation stage. A LabVIEW-based software program integrates the imaging and spectroscopy systems with online display of spectroscopic information while the system scans each pixel position. The software also allows for integrating the image intensity of all 15 channels to increase the signal-to-noise ratio by a factor of ~4 relative to single channel image. The integrated imaging and spectroscopy system produces essentially 4-D data in which spatial data are along 2 dimensions, spectral data are in the 3rd dimension, and time is the 4th dimension. The system performance was tested by collecting imaging and spectral data with a 7.5-cm-diameter and 1m long gas cell in which test chemicals were introduced against a liquid nitrogen background.

Keywords: passive millimeter waves, single pixel imaging, chemical spectroscopy

1. INTRODUCTION

Passive millimeter wave (MMW) techniques have been in use for remote sensing of the Earth's surface and its atmosphere. The underlying principle is the measurement of Planck's blackbody radiation of materials at millimeter wavelengths. The main advantage of passive MMW imaging is that it can provide ground target information under all weather conditions; optical systems (visible and IR), on the other hand, require clear atmospheric conditions for reliable operation. For example, the atmospheric attenuation in the range of MMW frequencies is 0.07 to 3 dB/km in drizzle and fog conditions, whereas it is one to three orders of magnitude higher at optical frequencies (exceeding 100 dB/km in foggy conditions).[1,2] In addition, the MMW technique offers better thermal contrast of objects because of emissivity differences of objects at these wavelengths. Image contrast is especially better in outdoor environments owing to cold sky reflected radiation. For example, the apparent temperature of the sky at 94 GHz is 70K in comparison to 220K at infrared wavelengths. Because of reflectivity variations of common objects for millimeter waves (metal ~1, water 0.6, wood 0.6, and concrete 0.2), the MMW sky reflected radiation offers better thermal contrast than at infrared wavelengths. More important, signal "washouts" do not occur since the apparent temperature between the background and object will rarely be equal.

In addition to imaging, passive millimeter waves can be used to obtain spectroscopic signature of chemicals. Passive MMW spectroscopy has been used in radio telescopes for studying the composition of interstellar gases as well as in monitoring the water and oxygen profiles in the atmosphere. With a 15-channel filter bank in the 146-154 GHz RF band, we have recently measured the 150 GHz line of nitric oxide from a test stack at a distance of 600 m from the radiometer.[3]

The objective of this paper is to develop an integrated imaging and spectroscopy system for broad area search and detection of nuclear facilities. While imaging can provide broad area search of facilities for certain observables such as structural changes, traffic, and effluent heat, the spectroscopic system can provide more specific signature of effluent chemicals from exhaust stacks. Millimeter wave radiation allows for rotational spectroscopy of polar molecules, so it can provide fingerprint signatures of polar chemicals emanating from material processing facilities.

2. SINGLE PIXEL IMAGER

Passive MMW imagers can be either a raster scanned type using a single detector or a focal plane imaging type with an array of detectors (similar to CCD or CMOS optical imagers).[4-6] Single detector imaging, also called single-pixel imaging, allows for the use of one-of-a-kind detector, but real-time imaging is generally not practical because of the point-by-point mechanical scanning required for this system. Focal plane array imaging, although suited for real time, is complex and expensive at mm wavelengths because the number of antennas/detectors that can be incorporated in the focal plane space is physically limited.

Because we already have an advanced spectroscopic receiver, we chose to retrofit the spectroscopy system with a single-pixel imaging accessory. There are many types of a single pixel imager based on: (i) object scanning, (ii) mirror or lens scanning, and (iii) aperture coding (spatial light modulation). It is also possible to scan the receiver but the cable noise during movement can adversely affect the data. We chose to use lens scanning approach because it allows for moving the field of view across the target without causing any interference to the spectroscopy system.

2.1 Lens scanning

Consider an imaging lens of diameter D and focal length f and an object at a distance R from the lens (see Fig. 1). The angular width of the beam θ in radians is:

$$\theta = \frac{\lambda}{D}, \tag{1}$$

where λ is the wavelength.

The spot size A of the beam at distance R is

$$A = R\theta \tag{2}$$

The angular shift of beam spot for a lateral/vertical shift of lens by a distance y from the center is

$$\phi = \arctan(\frac{y}{f}) \tag{3}$$

The shift in beam spot Y along the lateral/vertical dimension of the target at distance R equals

$$Y = (y/f)R \tag{4}$$

An offset y of lens from the center of the detector, therefore, causes a shift Y of the beam spot from the center of the target; the field of view at the object at distance R for a $2y$ by $2y$ scan of the lens is $2Y$ by $2Y$.

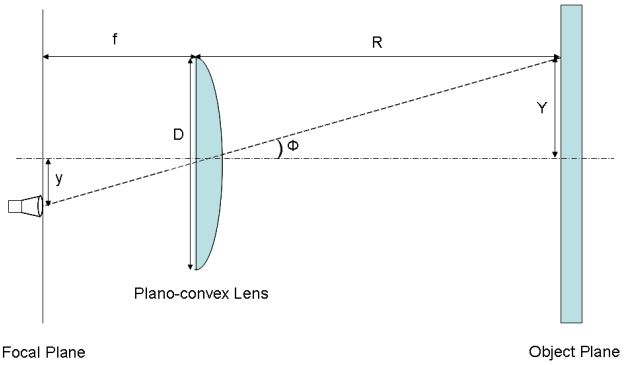

Figure 1. Schematic diagram of imaging system with lens scanning.

We mounted a 15-cm-imaging lens on a scanning stage and tested the image formation. Figure 2 gives a pictorial view of the lens scanning system. The corrugated scalar horn is at or near the focal plane of the lens; the distance between the lens and feed horn is optimized, depending on the target distance, to form sharp images. Figures 3(a) gives the lens scanned images of a pair of scissors for 15 spectral channels; the pixel size is 0.5 mm and the integration time is 1s. All channels give near identical results, showing that the spectral channels respond similarly (with the exception of their gains and offsets) and that there is no spectral variation in the target signal, as expected. Compared to individual images obtained with a detection bandwidth of 500 MHz, the summed image simulating a 7.5GHz radiometer bandwidth increases the signal-to-noise ratio (SNR) as seen in Fig. 3(b). The smallest feature of the object is the width of the handles (~5 mm), which is clearly resolved.

Figure 2. MMW imager setup, showing radiometer, imaging lens on scanner, and object.

2.2 Imager performance

Radiometer sensitivity is given by: [7]

$$\Delta \mathrm{T} = \frac{T_N}{\sqrt{B\tau}}, \tag{5}$$

where ΔT is minimum detectable temperature, T_N is noise temperature of the receiver, B is the pre-detection bandwidth, and τ is the post-detection integration time. The radiometer sensitivity is sometimes stated as noise equivalent difference temperature (NEDT), which is the minimum difference in temperature of a target that the imager can sense with a signal-to-noise ratio of unity.

$$NEDT = \frac{(NEP)\sqrt{B_v}}{(\partial P/\partial T)}, \tag{6}$$

where NEP is the noise equivalent power of the receiver in W/$\sqrt{Hz}$, B_v is the video bandwidth of the receiver=1/τ in which τ is the integration time, and $\partial P / \partial T$ is the rate of emission power with respect to temperature of the target. Using $NEP=k_B T_N \sqrt{B}$ and $P=\eta k_B TB$ in which k_B is Boltzmann's constant and η is the efficiency of the collection optics,

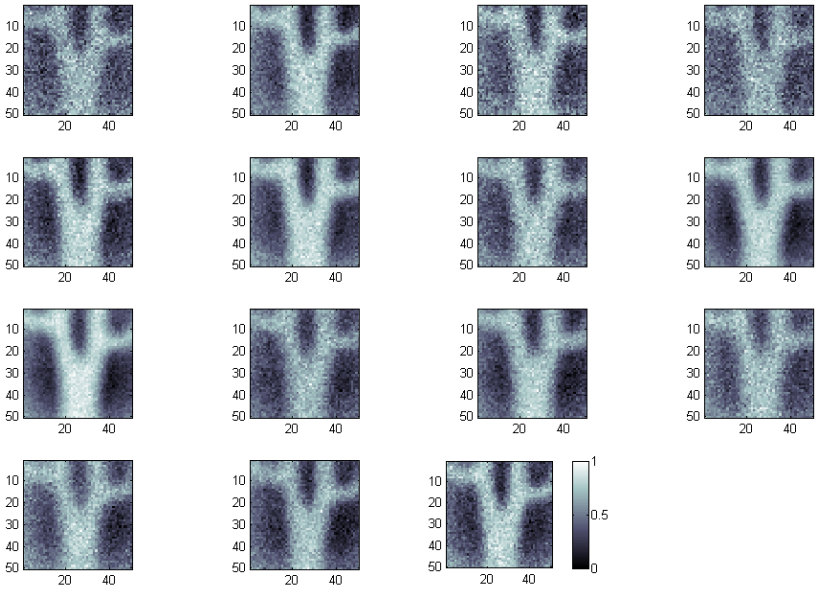

(a)

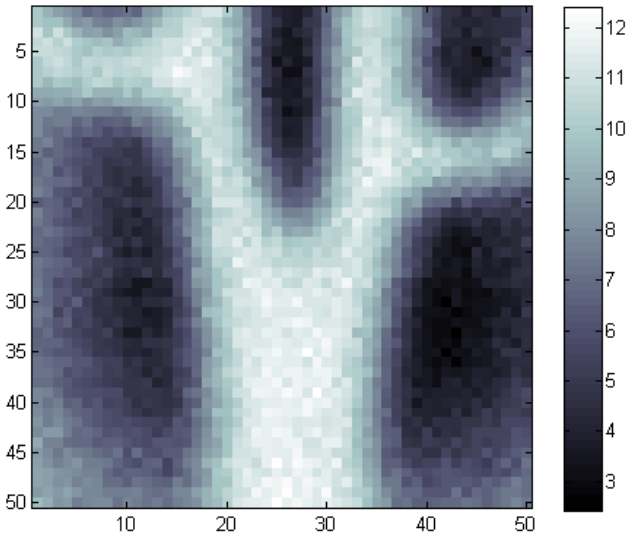

(b)

Figure 3. Images of a pair of scissors with lens scanning with pixel size 0.5 mm and integration time 1s: (a) multispectral images, (b) sum of normalized images, showing high SNR.

$$NEDT = \frac{T_N}{\eta\sqrt{B\tau}} = \frac{\Delta T}{\eta}. \quad (7)$$

In Table I, we give the performance metrics for two cases: (a) existing system for near range imaging and (b) a prototype system that is being modified for remote sensing.

Table 1. Imager performance metrics for the lens scanning 150 GHz radiometer.

System Parameter	Current system	Prototype system
Noise Figure	11.9 dB (SSB)	8 dB (DSB)
Noise temperature	4201K	1540K
Bandwidth	500 MHz	8 GHz
Integration time	0.5 s	1 ms
NEDT	0.38K	0.77K
Aperture size	15 cm	30 cm
Object distance	37 cm	1000 m
Object resolution	0.49 cm	6.6 m
Field of view	3.42 cm	167 m
Image pixels	28 x 28	100x100
Imaging speed/frame	397 s	10.3 s

3. INTEGRATED IMAGING AND SPECTROSCOPY SYSTEM

The imaging and spectroscopy parts of the system were integrated in LabVIEW program with the following features:

(i) 2-axis control of the scanning unit
(ii) Display of image formation for any channel or the averaged image from 15 channels while scanning; the averaged image shows target image with high SNR
(iii) Online display of spectral graph for each pixel; this give spectral information for each pixel
(iv) Introduction of hot and cold loads for calibration before, during, or after scanning
(v) Ability to save images of all spectral channels for post processing

The integrated imaging and spectroscopy system was tested using a gas cell setup in Fig. 4. The target scene consists of a 1m long gas cell with 7.5 cm ID and 8cm OD against a liquid nitrogen background. The gas cell is fitted with vacuum and feed lines; a test chemical may be introduced into the gas cell at a desired pressure from 10 mTorr to 1 atm.

Figure 5 gives the imaging and spectroscopy data for acetonitrile (CH_3CN) vapor at different pressures. A 10x10 image was obtained for each spectral channel with 4s integration time per pixel. The time sequence of tests consisted of (i) normalizing all 15 channels using cold (absorber immersed in liquid nitrogen) and hot (absorber at ambient temperature) loads, (ii) vacuum cell in the 1st row, (iii) pure CH_3CN at 2 Torr in rows 2-4, (iv) pure CH_3CN at 4 Torr in rows 5 and 6, (v) pure CH_3CN at 11 Torr in rows 7 and 8, (vi) air added to 11Torr CH_3CN to bring the total pressure to 740 Torr in row 9, and (vii) vacuum in row 10. The composite graph consists of individual images for the 15 spectral channels at the top and spectral plots of acetonitrile at the bottom. The images of channels are numbered 1 to 15 starting at the top row of images, which correspond to a center frequency of 146.75 GHz for Ch# 1 and increasing at 0.5 GHz interval to 153.75 GHz for Ch#15. The images show the circular part of the gas cell wall in all channels. Note that the spectrum of CH_3CN

peaks around 146 GHz, so the image of CH_3CN is seen predominantly in the lower numbered channels depending on the extent of pressure broadening. The 11 Torr image is brighter than that of 4 Torr because of increased concentration and the 740 Torr image is weaker because of dilution with nitrogen and it is spread into more channels starting from Ch#1 because of pressure broadening. The spectral plots include simulated line at 4 Torr from JPL data base and the measured spectral plots at pressures 4, 11, and 740 Torr. The measured plot averaged the data from several pixels at same pressure. The simulated and measured data at 4 Torr agree very well; the error bar is the standard deviation of intensity data from the pixels of same pressure. The pressure broadening effect is seen from the plots for 11 and 740 Torr.

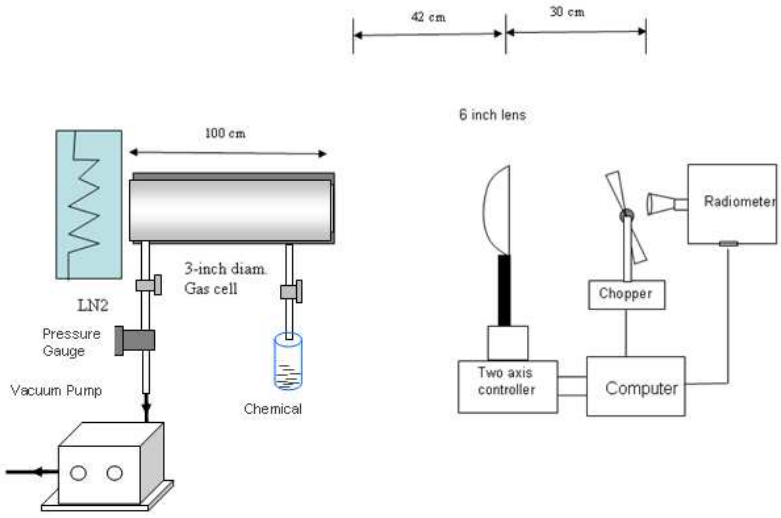

Figure 4. Imaging and spectroscopy test setup.

4. CONCLUSIONS

We have developed an integrated imaging and spectroscopy system in the passive MMW band of 146-154 GHz. The spectroscopy system uses 15 spectral channels, each 0.5 GHz wide. While imaging, the data channels are summed up in software to provide an imaging performance that is equivalent of wide RF bandwidth (7.5 GHz). At the same time, the spectral line of the target is displayed as each pixel is scanned. If the target is a solid material, the spectral line will be nominally flat. On the other hand, if it is a gaseous chemical possessing an absorption/emission line in the RF band, the corresponding spectral shape will be displayed.

Images of objects such as a pair scissors were obtained with all 15 channels with good image clarity. When we normalized the individual images of 0.5GHz bandwidth channels and summed them up from all 15 channels, the image contrast was equivalent to that of a 7.5GHz bandwidth radiometer with improved image quality. We analyzed and projected the imager performance metrics for remote sensing application. With a 30-cm imaging aperture, the passive MMW system is capable of imaging from 1 km away a 170m x 170m scene in 10 s with following features: image size 100 x 100, spatial resolution 7 m, and NEDT 0.8K.

We tested the integrated imaging and spectroscopy system by introducing acetonitrile vapor in a gas cell. The test data showed image of the solid parts of gas cell wall as well as the emission spectra of the gas inside the cell. The brightness temperature of the gas varied for each channel, depending on the strength of the emission line at the channel's frequency band. The measured spectral line agreed well with the simulated data of acetonitrile from JPL data base. The integrated data show the potential of imaging the location of an emission stack and obtaining the spectra of effluent gasses from it.

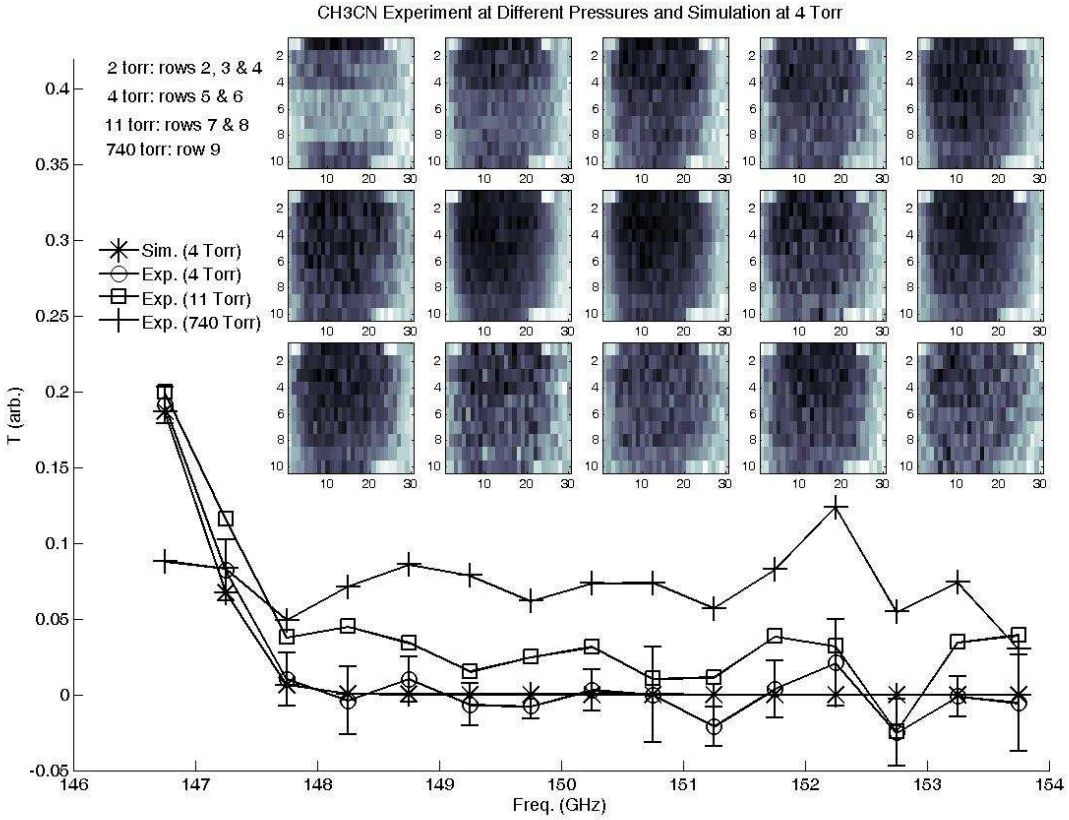

Figure 5. 3-D images of acetonitrile in a gas cell at different pressures.

Acknowledgements

This work is supported by the office of Nonproliferation and Verification Research and Development under the National Nuclear Security Administration of the U.S. Department of Energy under Contract No. DE-AC02-06CH11357.

REFERENCES

[1] Yujiri, L., Shoucri, M. and Moffa, P., "Passive millimeter-wave imaging," IEEE Microwave Magazine, September (2003).

[2] Appleby R. and Anderton, R. N., "Millimeter-wave and submillimeter-wave imaging for security and surveillance," Proc. IEEE, 95, 1683-1690 (2007).

[3] Gopalsami, N., Bakhtiari, S., Elmer, T. and Raptis, A. C., "Application of Millimeter-Wave Radiometry for Remote Chemical Detection," IEEE Trans. on Microwave Theory and Techniques, 56, 700-709 (2008).

[4] Lettington, A. H., Dunn, D., Attia, M. and Blankson, I. M., "Passive millimeter-wave imaging architectures," J. Optics A: Pure and Applied Optics, 5, S103-S110 (2003).

[5] Fetterman, M. R., Grata, J., Jubic G., Kiser, Jr., W. L. and Visnansky, A., "Simulation, acquisition, and analysis of passive millimeter-wave images in remote sensing applications," Optics Express, 16, 20503-20515 (2008).

[6] M. Duarte, M. Davenport, D. Takhar, J. Laska, T. Sun, K. Kelly, and R. Baraniuk, "Single-pixel imaging via compressive sampling," *IEEE Signal Processing Magazine*, 25(2), pp. 83-91, March 2008.

[7] Janssen, M. A. (ed.), [Atmospheric Remote Sensing by Microwave Radiometry], John Wiley and Sons, New York (1993).